NUMERICAL INVESTIGATION OF BOILING

M. Sagan and S. Tanguy* and C. Colin
*Author for correspondence
Institute of fluid mechanics of Toulouse
Toulouse, 31400, France
E-mail: msagan@imft.fr, tanguy@imft.fr, colin@imft.fr

ABSTRACT

In this work, we study different phenomena that occur during nucleate boiling. We numerically investigate boiling using two phase flow direct numerical simulation based on a level set / Ghost Fluid method. This method allows us to follow the interface and to make accurate geometric calculation as for bubble curvature. Nucleate boiling on a plate is not only a thermal issue, but also involves multiphase dynamics issues at different scales and at different stages of bubble growth. As a consequence, we divide the whole problem and investigate separately the different phenomena considering their nature and the scale at which they occur.

First we analyse the boiling of a static bubble immersed in an overheated liquid. We perform numerical simulations at different Jakob numbers in the case of strong discontinuity of density through the interface. These simulations permit us to estimate the accuracy of our numerical method dealing with phase change in the context of two phase flow direct numerical simulation. The results show a good agreement between numerical bubble radius evolution and the theoretical evolution found by Scriven (1959). The validation of our code for the Scriven case allows to pursue our study by focusing on the phenomena that take place in the particular case of an interaction with a wall. This interaction is characterised by the angle formed between a solid and a fluid interface, named the contact angle. We implement a method that makes it possible for a droplet, to reach, in the case of a static contact angle, a steady state corresponding to a theoretical equilibrium. Besides this method enables to take into account the contact angle hysteresis model, which considers different angles whether the contact line is advancing or recoiling. We perform simulations of the spreading of a liquid droplet impacting on a plate, and we compare the maximum spreading diameter and the advancing and receding droplet behaviour of our numerical results with the experimental data Son and Lee (2010) have reported.

INTRODUCTION

Generally speaking, for pool boiling we identify several mechanisms involved in different degrees, depending on properties of the fluids and on boiling conditions. In numerical study we usually focus on two main mechanisms.

■ Evaporation over the bubble: Usually during boiling, a thermal layer forms over the plate that can cover a part of the bubble, as a result a thermal transfer occurs when the temperature of the liquid in the thermal limit layer is over the saturated temperature. This mechanism does not imply particular physical difficulties, and is fully described by classical thermal equations that will be presented in next section. Nevertheless simulation of this mechanism meets the numerical challenge of having good estimation of discontinue variables derivatives.

■ Micro-layer evaporation and three phase contact line evaporation: During bubble growth, a thin liquid film is trapped under the bubble, due to microscopic interactions and to the difference between velocity of growth and velocity of de-wetting. Evaporation of this micro layer contributes to the bubble growth. At the level of the three phase contact line a singularity occurs and makes the heat flux diverge. Some authors, as Stephan and Busse (1992), resolved this singularity by assuming the presence of an adsorbed film at the smallest scales where thermal heat transfer is limited by an interfacial resistance.

Since nucleate boiling is a complex phenomenon to compute, we decided to devided the whole problem and to investigate seperately heat and mass transfer around the bubble and wall interaction effects. First, we are going to analyse the vaporisation of a static bubble immersed in an overheated liquid, then we will consider hydrodynamic aspects involved in wall-interface interaction while bubble grows on a surface, but before let us present our numerical method.

GOVERNING EQUATIONS AND NUMERICAL METHOD

The code used for our simulation, named DIVA, is developed by Tanguy (2004) at IMFT(Institute of fluid mechanics of Toulouse), and allows simulation of multi phase flows in the framework of atomisation or vaporisation, as Tanguy et al. (2007) have showed. In this code the interface is tracked thanks to a level set method. This method is based on a scalar distant function (represented by $\Phi(x,y,z)$), that is superior than zero in the liquid phase and inferior in the vapour phase, as a result The interface is represented by the level line zero, defined by $\Phi(x,y,z)=0$. The interface motion is taken into account thought an advection equation (1) which transports all the different level lines by the local velocity field $\mathbf{u}$.

$$\frac{\partial \Phi(x,y,z)}{\partial t} + \mathbf{u}\cdot\nabla\Phi(x,y,z) = 0 \tag{1}$$

To make sure that the level set function remains a distance function we use an algorithm of re-initialisation. At every time step, we perform an internal iteration on τ (see equations 2 to 3)

$$\frac{\partial d}{\partial \tau} = sign(\Phi)(1-|\nabla d|) \tag{2}$$

$$sign(\Phi) = \begin{cases} -1 & \Phi < -dx \\ \frac{\Phi}{\sqrt{\Phi^2+dx^2}} & |\Phi| < dx \\ 1 & \Phi > -dx \end{cases} \qquad d(x,t,\tau=0) = \Phi(x,t) \tag{3}$$

In equation 2, τ is the internal iterative parameter and $d(x,t,\tau=0)$ corresponds to the level set at the time step, t, considered. As so, by iterating on τ we can re-initialise the level set function without changing the level line zero which is the interface, one can find more details on this algorithm in Sussman et al. (1994). In DIVA the Navier Stokes equations and energy balance equation are solved for incompressible flow in each phase and the connection between each phase is ensured thanks to the jump conditions at the interface. If $\mathbf{u}$ is the velocity field, P the pressure, σ the surface tension, κ the curvature, the equations considered for liquid and for vapour, are the following: (4),(5),(6), and for the jump conditions we considered the following equations : (7),(8),(9).

$$\rho(\Phi)(\frac{\partial \mathbf{u}}{\partial t} + (\mathbf{u}\cdot\nabla)\mathbf{u}) = -\nabla P + \rho(\Phi)\mathbf{f_{vol}} + \nabla\cdot(\mu(\Phi)(\nabla\mathbf{u}+\nabla^T\mathbf{u})) \tag{4}$$

$$\nabla\cdot\mathbf{u} = 0 \tag{5}$$

$$\rho(\Phi)c_p(\frac{\partial T}{\partial t} + (\mathbf{u}\cdot\nabla)T) = \nabla\cdot(k\nabla T) \tag{6}$$

Jump conditions at the interface:

- For energy (with $\dot{m}$ the mass flux and L the latent heat of vaporisation):

$$[-k\cdot\nabla T\cdot\mathbf{n}_{interf}]_\Gamma = \dot{m}L \tag{7}$$

- For mass:

$$[\mathbf{u}\cdot\mathbf{n}_{interf}]_\Gamma = \dot{m}\left[\frac{1}{\rho}\right]_\Gamma \tag{8}$$

- For momentum:

$$[P]_{\Gamma_{v-l}} = \mathbf{n}_{interf}\cdot[\mu(\nabla\mathbf{u}+\nabla^T\mathbf{u})]_{\Gamma_{v-l}}\cdot\mathbf{n}_{interf} + \sigma\kappa - \dot{m}^2(\frac{1}{\rho_v}-\frac{1}{\rho_l}) \tag{9}$$

We solve the momentum balance thanks to the projection method to impose incompressibility in each phase. First, we compute an intermediate velocity equation (10), to solve this equation we use a Runge Kunta of order 2 for the temporal derivatives and a WENO5 scheme for the spatial derivatives of the convective term, as it has been done by Jiang and Shu (1996). Using the intermediate velocity one computes equation of Poisson for the pressure equation (11) using volume finite scheme of second order, then we obtain the real free divergence velocity, equation (12)

$$\mathbf{V}^* = \mathbf{V}^n - \Delta t[(\mathbf{V}^n.\nabla)\mathbf{V}^n - \frac{\nabla(\mu^n(\Phi)(\nabla\mathbf{u}^n+\nabla^T\mathbf{u}^n))}{\rho^n(\Phi)}] \tag{10}$$

$$\nabla.\left(\frac{\nabla P^{n+1}}{\rho(\Phi)}\right) = \frac{\nabla.\mathbf{V}^*}{\Delta t} \tag{11}$$

$$\mathbf{V}^{n+1} = \mathbf{V}^* - \Delta t\frac{\nabla P^{n+1}}{\rho(\Phi)} \tag{12}$$

Besides the level set method, to trait properly the jump conditions at the interface we use a ghost fluid method. For many fields, the interface is a zone of discontinuity which makes, for instance, calculation of derivatives inaccurate. The ghost fluid method, which has already been tested for simulation of multiphase incompressible flow by Kang et al. (2000), consists in considering a ghost domain where we extend the different variables. As a result, for a variable f, we consider points of f defined in phase 1 to extent the field with ghost points in phase 2. We do the same thing with the points defined in phase 2. Then we evaluate the jump due to the discontinuity: $[f]_\Gamma$. Considering these methods, we can impose all the jump conditions from equations : (7),(8),(9). Let us note that in the case of boiling, it is important to have a good estimation of the thermal gradient jump, which is at the origin of the mass flux that controls bubble growth. To evaluate the Jump condition for the energy balance, we use a second order method to expand the temperature field, that Aslam (2004) has used.

However the originality of our method consists in considering an additional algorithm to impose the free divergence. The use of the ghost fluid method implies extension of the different variables in ghost domain. The extension of the velocity field usually causes parasitic currents. To minimise this phenomenon, instead of calculating directly a ghost gas velocity $\mathbf{V_l} + \dot{m}\left[\frac{1}{\rho}\right]_\Gamma$ we solved equation (10) and (11) and compute a ghost pressure for the gas in the liquid domain equation (13), then from this ghost pressure we obtain a ghost gas velocity (see equation (14)). The reader can find more details on this method in the publication of Tanguy et al. (2007).

$$\nabla \cdot (\frac{\nabla P^{ghost}}{\rho^{n+1}}) = \frac{\nabla . \mathbf{V_g^*}}{\Delta t} \tag{13}$$

$$\mathbf{V_g^{ghost}} = \mathbf{V_g^*} - \Delta t(\frac{\nabla P^{ghost}}{\rho^{n+1}}) \tag{14}$$

Next, using our numerical tool, we propose to consider separately the different physical phenomena. So, in a first time we analyse the vaporisation of a static bubble immersed in an overheated liquid.

GROWTH IN A LIQUID AT REST - THEORETICAL RESULTS OF SCRIVEN

In this part we propose to analyse bubble growth in an overheated liquid at rest. Without bubble motion both the velocity and thermal fields around the bubble are spherically symmetrical and has been theoretically determined by Scriven (1959). Besides in the case without motion, the thermal transfer around the bubble can be fully characterised by the Jakob number.

$$Ja = \frac{\rho_l c_{pl}(T_\infty - Tsat)}{\rho_v L} \tag{15}$$

Jackob number compares the sensitive heat with the latent heat and informs about the quantity of energy by volume unit which can be provided by the liquid for phase change. The more important the Jakob number is, the faster will be the phase change, and the thinner thermal boundary layer will be as Legendre et al. (1998) have showed. As a result to evaluate our numerical tool, it is interesting to perform several simulations for various Jakob numbers. Consequently, a parametric study has been made on the mesh size, for different Jakob numbers.

The results are presented in table 1. These simulations are initialised with a bubble of radius $R_0 = 1mm$. The main results of the theoretical analysis of Scriven (1959) that will be used for comparison with our simulations are presenting in equations: (15), (16), (17),(18). Scriven found that the time evolution of the bubble radius is given by equation (16) :

$$R = 2\beta\sqrt{\kappa t} \tag{16}$$

Where κ is the thermal diffusivity, and β is an adimensional parameter that characterises the growth rate and that is solution of an implicit equation that can be solved numerically with equation (17)

$$Ja = -2\beta^3 \cdot exp(\beta^3 + 2\epsilon\beta^2) \cdot \int_\beta^\infty \frac{exp(-x^2 - 2\epsilon\frac{\beta^3}{x})}{x^3} dx \tag{17}$$

with ϵ given by equation (18)

$$\epsilon = 1 - \frac{\rho_v}{\rho_l} \tag{18}$$

The temperature field is obtained by equation (19)

$$T(r) = T_\infty - \frac{T_\infty - -T_{sat}(P_\infty)}{Ja} g(\beta) f(\beta, \frac{r}{2\sqrt{\kappa t_0}}) \tag{19}$$

with r the radial coordinate, and g and f defined respectively by equation (20) (21)

$$g = 2\beta^3 exp(\beta^2(1-\beta\epsilon)) \tag{20}$$

$$f(\beta, s) = \int_s^\infty \frac{exp(-x^2 - 2\epsilon\frac{\beta^3}{x})}{x^3} dx \tag{21}$$

GROWTH IN A LIQUID AT REST - SIMULATION AND DISCUSSION

Thanks to the theoretical solution of Scriven (1959), we determine for each case, the time corresponding to an increase of a factor 2 on the bubble radius, and we compare the radius expected with the radius obtained. The simulations are performed for liquid-vapour water with properties taken in the standard conditions at 1 atmosphere, but to decrease time step, viscosities are divided by 10∗.

Second order extension with correction for divergence free								
Jakob :	3	4	5	6	7	8	9	10
Mesh	Relative error on the final radius (%)							
64x128	9.3	15	21	26.2	30.5	33.8	36.6	38.7
128x256	1.4	1.6	2.8	5.0	7.9	11.5	14.4	17.6
256x512	1.0^+	0.4	1	1	0.5	0.5	1	2

Table 1: *Second order extension with correction for divergence free*

∗In table 1, we observe good convergence properties when mesh size is refined, first order when thermal boundary is roughly resolved (meaning that when the mesh size is divide by 2 the error is also divide by 2^1), and higher order (upper than 2), when thermal boundary is sufficiently resolved. During our study we observed that these good properties was directly linked to the high order method used to extend the temperature field, (see publication of Aslam (2004)).

In figures 1 to 4, we present the pictures obtained with our simulations for time, $4t_0$ (where t_0 corresponds to a radius of $R_0 = 1mm$ for the theoretical solution, and $4t_0$ corresponding to a radius of 2 mm for the theoretical solution), for two Jakob numbers (3 and 10) in the case of a mesh corresponding to 256x512. We performed our simulations in a box with a width $Lr = 6R_0$ and a length $L_z = 12R_0$

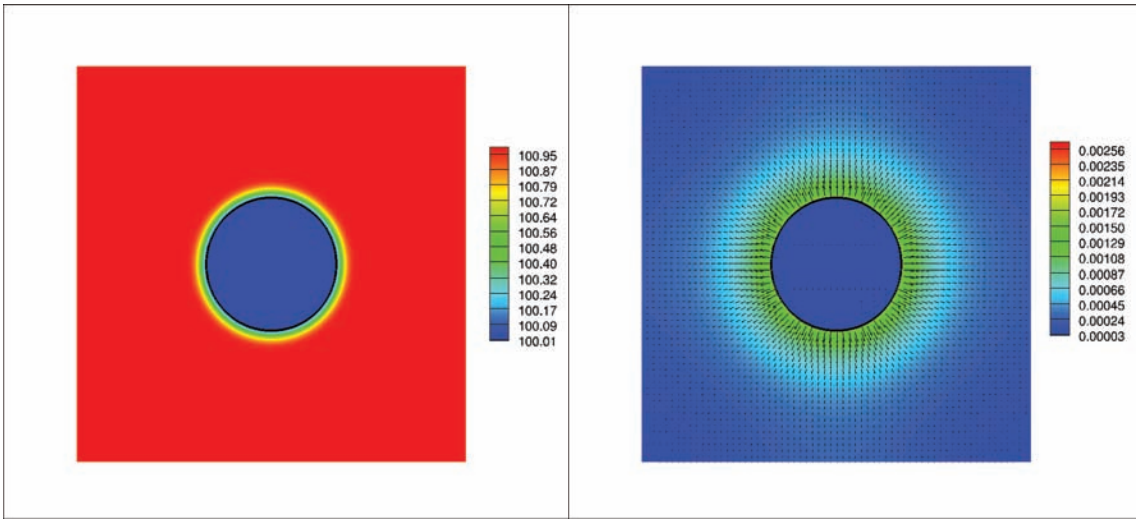

Figure 1: *Thermal field* $(°C)$ *at* $4t_0$, *Ja=3*

Figure 2: *Velocity magnitude* m/s *at* $4t_0$, *Ja=3*

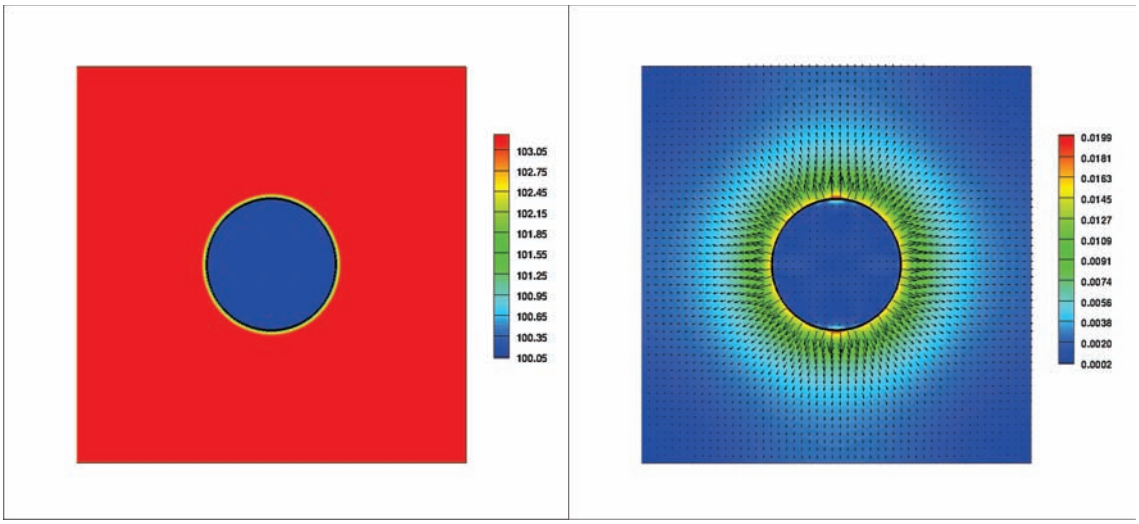

Figure 3: *Thermal field* $(^{\circ}C)$ *at* $4t_0$*, Ja=10*

Figure 4: *Velocity magnitude* m/s *at* $4t_0$*, Ja=10*

we display in colour the thermal field in pictures (1,3), and the velocity magnitude field in fig.2, and fig.4. We can see that the dynamic boundary layer is controlled by the radial convection. Besides, by watching the scale length for velocity vector for the two Jakob numbers, it points out how the value of the Jakob number characterises the radial flow. The more it is important and the more the radial velocity magnitude is. Besides, we can see also the impact of the Jakob number on the thickness of the thermal boundary layer. As we said before the bigger the Jakob number is the thinner the thermal boundary layer will be. This explains why, for one mesh size the relative error increases with the Jakob number (1). This is due to the fact that when the Jakob number increases thermal boundary layer resolution decreases. The evolution of the bubble radius versus time is plotted for the different meshes for Ja=10 (fig. 5) and Ja=3 (fig. 6)

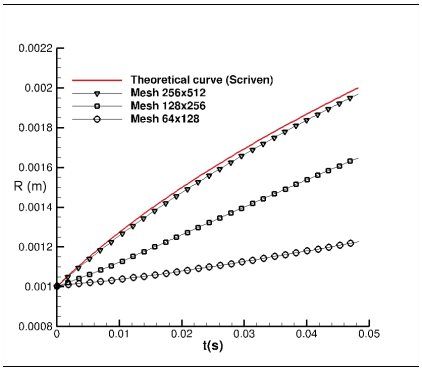

Figure 5: *Evolution of the radius for Ja=10 with different mesh sizes*

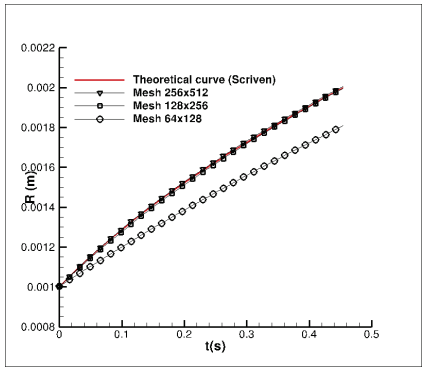

Figure 6: *Evolution of the radius for Ja=3 with different mesh sizes*

As we can see on fig 5,6, considering the Jakob number, we have to be careful of the mesh used for our simulations. Also this parametric study indicates that to have a proper resolution we shall have at least 6 points in the thermal boundary layer. Considering this last element we can see that we obtain good results in agreement with the theoretical expectation.

The validation of our code for the Scriven test case allows us to pursue our study by focusing on the phenomena that take place in the particular case of interactions between wall and fluid surface. As a consequence in the next part we are going to investigate the physics that occurs near the contact line. Here also, rather than to directly attack the problem of evaporation of the micro layer, we choose to study at first the interactions between a plane surface and an interface in an isothermal case without phase change.

INTRODUCTION OF WALL ASPECT - MODEL FOR CONTACT ANGLE

The surface tension results of the sharp variation of density by passing from liquid to vapour. When we pass from fluid to wall, the physico-chemical variations lead to the creation of a surface energy. This energy has for consequence, in particular, to

deform the interface, also in the case of a drop (or of a bubble) laying on a wall, we define a contact angle, as the angle formed between the interface and the wall in the liquid side. In the static case without phase change some models, as the Young Dupré law can be used, that gives the value of the static contact angle versus the surface energies generated by interface liquid-solid, vapour-liquid and solid-vapour.

$$\sigma_{lv} cos(\theta) = \sigma_{sv} + \sigma_{sl} \qquad (22)$$

σ_{lv} surface tension liquid/vapour
σ_{sv} surface tension solid/vapour
σ_{sl} surface tension solid/liquid
θ contact angle

In the dynamic case the classical fluid mechanics description with the Navier Stokes equations, leads to a singularity on the velocity field at the contact line between the fluid interface and the wall. Indeed the condition of not sliding associated with an interface motion on the wall leads to infinite viscous constraint. To solve this singularity several descriptions were adopted. one approach, presented by Dussan (1976), consists in introducing a length of sliding Ls which authorises the interface to slide on the wall. In the static case, the static contact angle equation (22) is a coherent boundary condition. But it is not valid any more in the dynamic case in which, it is advisable to find a relation involving the contact angle and the speed of sliding of the contact line.

Actually, due to the characteristic size of the small scales, it is not possible to simulate the whole phenomenon occurring in the motion of the contact line that is responsible, for intense, of hysteresis (interval of angle $[\theta_r, \theta_a]$, in which the contact line does not move, see fig.7)

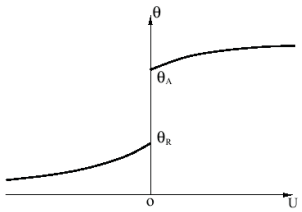

Figure 7: *Evolution of the contact angle with the velocity, picture takes form Legendre and Dupont (2009)*

To take into account the physics at the small scales we simply prefer to consider a law of variation connecting the dynamic contact line speed. So we impose alternately speed of sliding, and contact angle.

If $\theta_r < \theta < \theta_a$: The contact line does not move, and, if $\Phi(i, j, k)$ define the level set function we have $\Phi^{t+dt} = \Phi^t$

If $\theta_r \geq \theta$: The contact line moves, and we set $\theta = \theta_r$, and that implies in axisymmetric case, $\frac{\partial \Phi}{\partial z} = cos(\theta_r)$

If $\theta_a \leq \theta$: The contact line moves, and we set $\theta = \theta_a$, and that implies in axisymmetric case, $\frac{\partial \Phi}{\partial z} = cos(\theta_a)$

INTRODUCTION OF WALL ASPECT - STATIC ANGLE

Considering these previous elements we perform some simulations. The results obtained are gathered in the following pages. At first we consider the case without hysteresis, with the following boundary condition equation (23).

$$\theta = \theta_{eq} \qquad (23)$$

The parameters we used for this first study are in table:2:

variable	values	unity
liquid viscosity	0.00113	$Pa.s$
gas viscosity	0.0000178	$Pa.s$
liquid density	$1.07 \cdot 10^3$	kg/m^3
gas density	1.2	kg/m^3
surface tension	0.07	N/m

Table 2: Parameters of the simulation corresponding to water and air at atmospheric pressure

In this case, we consider a droplet initialised with a contact angle different form its static contact angle. When the simulation starts surface tension generates a movement of the interface, and the droplet evolves spontaneously towards the balance given by the previous equation (23). The shape of the drop at equilibrium, and the diameter of its base are calculated by neglecting gravity effects, then the equilibrium shape is a truncated sphere.

When the droplet reaches its equilibrium position we estimate its foot diameter and parametric study on mesh sizes is driven for two different static contact angles, $\frac{\pi}{3}$ see fig. 8 and $\frac{2\pi}{3}$ see fig. 9. The results are presented in table 3

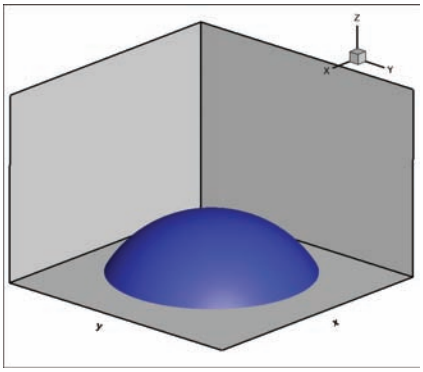

Error (%)		
Equilibrium angle	$\frac{\pi}{3}$	$\frac{2\pi}{3}$
Mesh (40x40)	7.4	5.4
Mesh (80x80)	3.7	3.2
Mesh (160x160)	1.8	2.1
Mesh (320x320)	0.9	1.1

Table 3: *Relative error for different meshes*

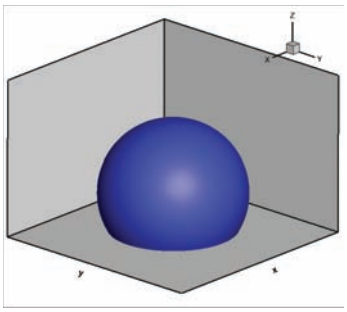

Figure 8: *droplet shape with* $\theta_{eq} = \frac{\pi}{3}$

Figure 9: *droplet shape with* $\theta_{eq} = \frac{2\pi}{3}$

Globally we observe that the obtained results are rather satisfactory. The drop reaches well its equilibrium position. Furthermore we also notice that when the mesh size is divided by two, we divide the error also more or less by two.

INTRODUCTION OF WALL ASPECT - SIMULATION OF DROPLET IMPACT

Let's us now consider the case with hysteresis. In the case of an impacting drop with a velocity of 0.285 $m.s^{-1}$, we can look at the oscillations of its spreading diameter around its equilibrium position. The numerical results are compared to those reported in Son and Lee (2010). In this case we consider a situation of hysteresis with a receding contact angle of 25°, and an advancing contact angle of 90°. All parameters used for the simulation are gathered in table 4. We observe the results obtained during our simulations (fig.10)

variable	value	unity
viscosity of the liquid	0.0032	$Pa.s$
viscosity of the gaz	0.0000178	$Pa.s$
density of the liquide	$1.07 \cdot 10^3$	kg/m^3
density of the gaz	1.2	kg/m^3
surface tension	0.035	N/m
droplet diameter	0.96	mm
velocity of impact	0.285	m/s
advancing contact angle	90	deg
receding contact anlge	25	deg

Table 4: Parameters of our simulations

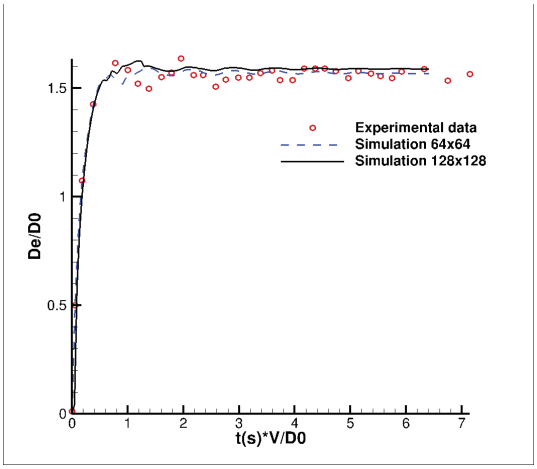

Figure 10: *Spreading diameter, comparison between experimental results used by Son and Lee (2010) and numerical results obtained with DIVA.*

First we can say that our simulations seem to be in good agreement with the experimental results reported in the publication of Son and Lee (2010). Actually it is interesting to note that the speed of the contact line during the spreading phase, found numerically, seems to correspond well to that presented in their publication. Nevertheless, this test case does not allow to study exactly the oscillatory regime. Indeed, the contact line slows down very quickly and oscillates only very weakly around its

equilibrium position. So, we should investigated the performance of our numerical method used to described the contact angle on other test cases with more important oscillatory regimes.

CONCLUSION AND PERSPECTIVES

The results obtained numerically are encouraging. Indeed, in the case of a bubble growth in an infinite overheated environment we observe a good agreement between the theoretical results and the results of our simulations. Besides the basic description used for the contact line seems sufficient to obtain a global behaviour that matches with some experimental observations.

So during the next step of our study, we will investigate more accurately the dynamics of the contact line. Then we will evaluate the method with thermal transfer at the wall by performing a parametric study on the heat flux near the contact line for different contact angle and for different wall superheats (see from fig. 11 to fig. 16). Then the possibility and the necessity of introducing a model of a contact angle that takes into account thermal effects will be investigated.

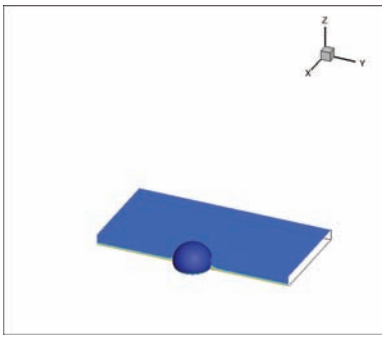

Figure 11: *Thermal field in the liquid and heat flux on the bubble shape at* t_0

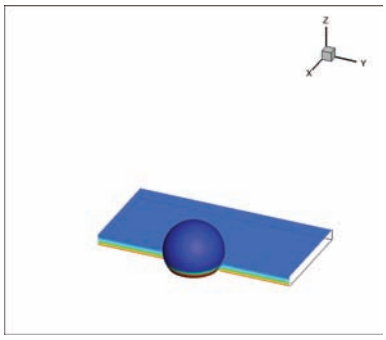

Figure 12: *Thermal field in the liquid and heat flux on the bubble shape at* t_1

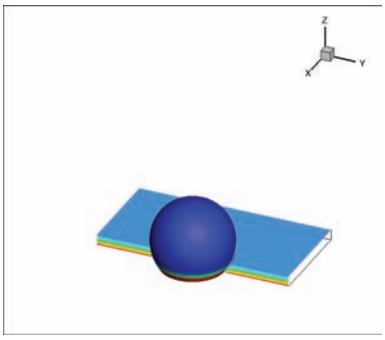

Figure 13: *Thermal field in the liquid and heat flux on the bubble shape at* t_2

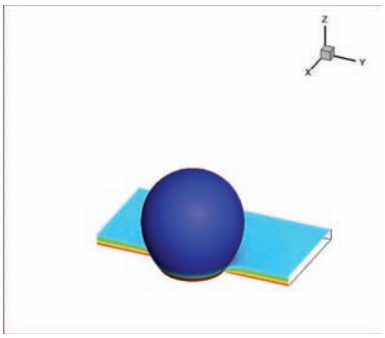

Figure 14: *Thermal field in the liquid and heat flux on the bubble shape at* t_3

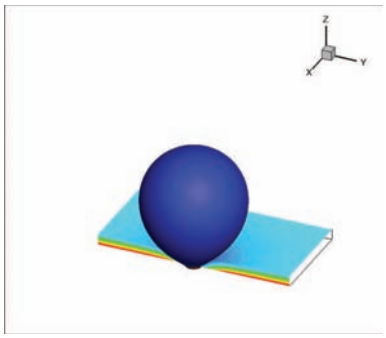

Figure 15: *Thermal field in the liquid and heat flux on the bubble shape at* t_4

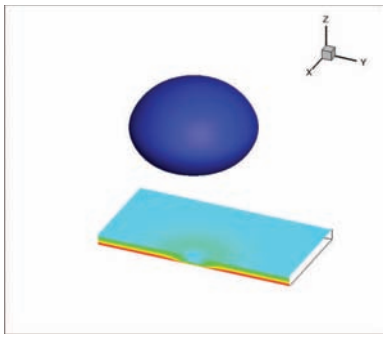

Figure 16: *Thermal field in the liquid and heat flux on the bubble shape at* t_5

ACKNOWLEDGEMENTS

The authors would like to thank the Centre National pour la Recherche Scientifique, and the Centre National d'Études Spatiales (french space agency) for funding this study in the frame of the COMPERE project on the management of propellants in launcher tanks.

References

Aslam, T. (2004). A partial differential equation approach to multidimensional extrapolation. *J. Comput. Phys.*, 193:349–355.

Dussan, E. B. (1976). The moving contact line: the slip boundary condition. *Journal Fluid Mech*, 77:665–684.

Jiang, G. and Shu, C. (1996). Efficient implementation of weighted essentially non -oscillatory schemes. *J. Comput. Phys.*, 126:202–228.

Kang, M., Fedkiw, R., and Liu, X.-D. (2000). A boundary condition capturing method for multiphase incompressible flow. *Journal of Scientific Computing*, 15:323–359.

Legendre, D., Borée, J., and Magnaudet, J. (1998). Thermal and dynamic evolution of a spherical bubble moving steadily in a superheated or subcooled liquid. *Physics of Fluids*, 10:1256–1272.

Legendre, D. and Dupont, J. (2009). Numerical simulation of static and sliding drop with contact angle hysteresis. *Journal of Computational Physics*, 229:2453–2478.

Scriven, L. E. (1959). On the dynamics of phase growth. *Chem. Engng Sci.*, 10:1–13.

Son, G. and Lee, W. (2010). Numerical study of droplet impact and coalescence in a microline patterning process. *Computers and Fluids*, 42:26–36.

Stephan, P. C. and Busse, C. A. (1992). Analysis of the heat transfer coefficient of grooved heat pipe evaporator walls. *Int. J. Heat Mass Transfer*, 35:383–391.

Sussman, M., Smereka, P., and Osher, S. (1994). A level set approach for computing solutions to incompressible two-phase flow. *J. Comput. Phys.*, 114:146–159.

Tanguy, S. (2004). *Developpement d'une méthode de suivi d'interface. Applications aux écoulements diphasiques*. PhD thesis, Université de ROUEN.

Tanguy, S., Ménard, T., and Berlemont, A. (2007). A level set method for vaporising two phase flows. *Journal of Computational Physics*, 221:837–853.